Supporting Information

Distinct Adsorption Behavior and Structures of Cell-Penetrating Peptides at a Model Lipid Membrane Interface: A Heterodyne-Detected Vibrational Sum Frequency Generation Spectroscopy Study

Subhadip Roy,†[ab] Mohammed Ahmed,†[ab] Aniruddha Adhikari,†[a] Erika Kinoshita,[ac] Satoshi Nihonyanagi,‡*[ab] and Tahei Tahara*[ab]

[a]Molecular Spectroscopy Laboratory, RIKEN, 2-1 Hirosawa, Wako, Saitama 351-0198, Japan

[b]Ultrafast Spectroscopy Research Team, RIKEN Centre for Advanced Photonics (RAP), 2-1 Hirosawa, Wako, Saitama 351-0198, Japan

[c]Department of Chemistry, Graduate School of Science, Kyoto University, Kitashirakawa Oiwake-cho, Sakyo-ku, Kyoto 606-8502, Japan

‡ Present address: Department of Chemistry, Institute of Pure and Applied Sciences, University of Tsukuba, 1-1-1 Tennodai, Tsukuba 305-8571, Ibaraki, Japan

*E-mail: nihonyanagi.satos.fu@u.tsukuba.ac.jp, nsatoshi@riken.jp, tahei@riken.jp

† These authors contributed equally to this work.

Table of contents

S1. Effect of water OH stretch signal on the lipid CH stretch mode

The $Im\chi^{(2)}_{eff}$ spectra in the CH stretch region at air/charged monolayer/H_2O interfaces can be affected by the low-frequency tail of the broad OH stretch band of interfacial water. Because the sign and amplitude of the OH stretch response depend strongly on the interfacial electrostatic environment, the superposed OH-band tail can alter the apparent amplitude of CH stretch features, particularly in the higher-frequency side of the CH stretch region.

To examine this effect, we measured $Im\chi^{(2)}_{eff,SSP}$ spectra for air/lipid/H_2O interfaces using a negatively charged DPPG monolayer, a positively charged DPTAP monolayer, and a mixed DPPG/DPTAP monolayer. Here, DPTAP denotes 1,2-dipalmitoyl-3-(trimethylammonium) propane chloride. As shown in Figure S1, the sign and amplitude of the broad OH stretch response change systematically as the interfacial electrostatic environment changes from negative to positive. Because the low-frequency tail of the OH stretch band extends into the CH stretch region, it affects the apparent amplitude of the ~2970 cm^{-1} band. As a result, the positive amplitude of the ~2970 cm^{-1} band, relative to the negative CH band at ~2880 cm^{-1}, decreases systematically from DPPG to the mixed monolayer and to DPTAP.

This trend supports our interpretation that the change in the ~2970 cm^{-1} feature observed in Figure 2 mainly reflects the contribution from the superposed OH-band tail, rather than a change in the intrinsic lipid CH_3 stretch response itself.

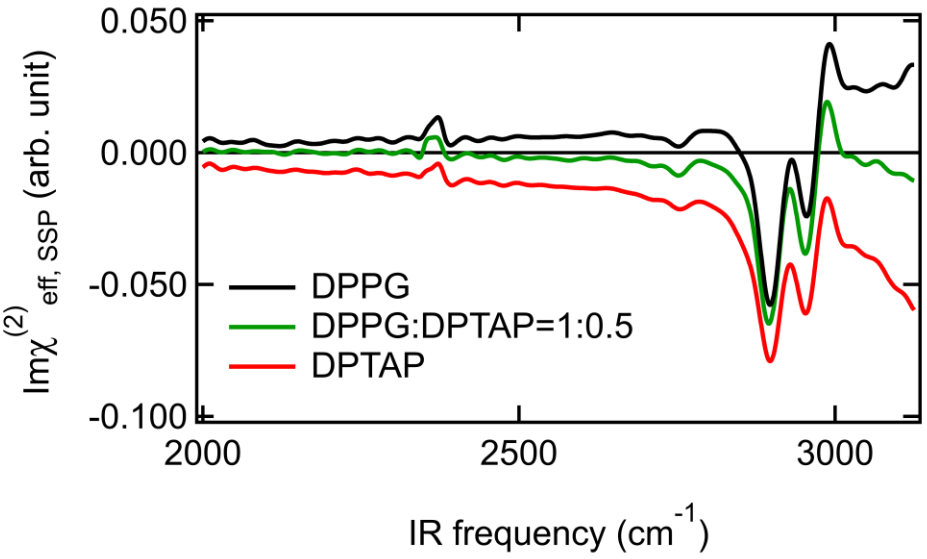

Figure S1. $Im\chi^{(2)}_{eff,SSP}$ spectra from the air/lipid/H_2O interface with DPPG (black), DPTAP (red), and a mixed DPPG/DPTAP (green) monolayers.

S2. $Im\chi^{(2)}_{eff,SSP}$ spectra at different SR8 concentrations

Figure S2 shows the $Im\chi^{(2)}_{eff,SSP}$ spectra of the air/DPPG/10mM Tris-HCl buffer (pD 7.4, D_2O) interface in the presence of 0.5 μM (orange) and 1.0 μM (blue) SR8 in the aqueous phase. As can be clearly seen, the intensity of the amide I band and the carbonyl stretch bands are comparable upon addition of 0.5 μM and 1.0 μM SR8, indicating that the adsorption of SR8 at the interface is already saturated at a concentration of approximately 0.5 μM.

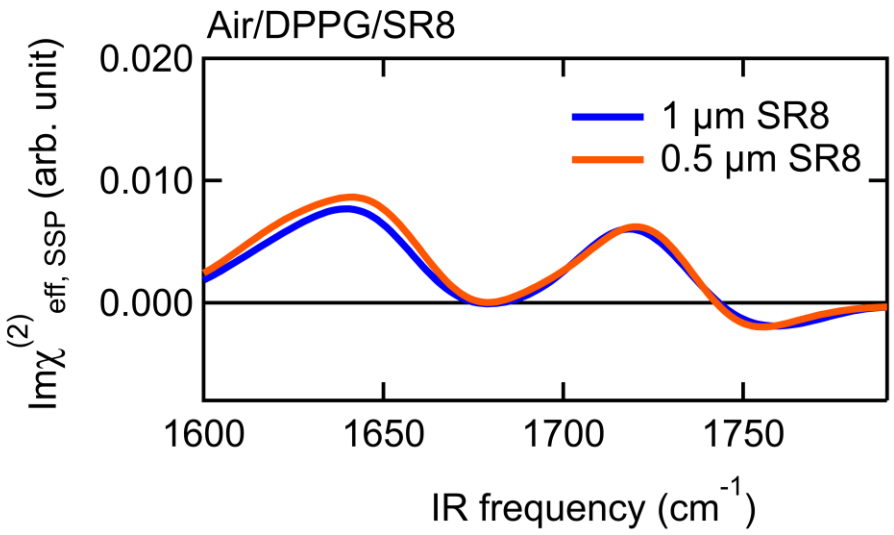

Figure S2. $Im\chi^{(2)}_{eff,SSP}$ spectra of the air/DPPG/10mM Tris-HCl buffer (pD 7.4, D_2O) interface in the presence of 0.5 μM (orange) and 1.0 μM (blue) of SR8 in the aqueous phase.

S3. Gaussian fitting analysis

The experimental $Im\chi^{(2)}_{eff}$ spectra (in SSP and PPP polarization combinations) of the air/DPPG/R8 and air/DPPG/SR8 interfaces in the C=O stretch region (Fig. 3 and Fig. 5 in the main text) contain contributions from the amide I band of the CPPs and carbonyl groups of the lipid molecules. To analyze the amide I band characteristics of the adsorbed CPPs, we fitted the $Im\chi^{(2)}_{eff}$ spectra of the air/DPPG/R8 and air/DPPG/SR8 interfaces using a combination of four and three Gaussian functions, respectively (as shown in Fig. 4 and Fig. 6 in the main text). The resulting best-fit parameters are listed in Table S1 and Table S2.

Table S1. Fitting parameters of the $Im\chi^{(2)}_{eff,SSP}$ spectra of the air/DPPG/R8 and air/DPPG/SR8 by four and three Gaussian functions, respectively.

Band	Assignment	Centre frequency (cm^{-1})	Band width (cm^{-1})	Amplitude
Air/DPPG/R8: Four Gaussian band fitting parameters				
I	Amide I	1643 ± 1	26 ± 0.6	0.0120
II	Amide I	1681 ± 1	25 ± 1.6	0.0079
III	Lipid carbonyl	1724 ± 0.2	20 ± 0.4	0.0125
IV	Lipid carbonyl	1761 ± 0.4	15 ± 0.5	-0.0032
Air/DPPG/SR8: Three Gaussian band fitting parameters				
I	Amide I	1641 ± 0.3	23 ± 0.4	0.0117
II	Lipid carbonyl	1725 ± 0.6	19 ± 0.8	0.0096
III	Lipid carbonyl	1760 ± 1.5	15 ± 1.9	-0.0033

Table S2. Fitting parameters of the $Im\chi^{(2)}_{eff,PPP}$ spectra of the air/DPPG/R8 and air/DPPG/SR8 by four and three Gaussian functions, respectively.

Band	Assignment	Centre frequency (cm^{-1})	Band width (cm^{-1})	Amplitude
Air/DPPG/R8: Four Gaussian band fitting parameters				
I	Amide I	1641 ± 1.4	20 ± 1.3	-0.0057
II	Amide I	1676 ± 1.8	21 ± 2.5	-0.0041
III	Lipid carbonyl	1722 ± 0.4	18 ± 0.9	-0.0055
IV	Lipid carbonyl	1757 ± 0.8	13 ± 1	0.0023
Air/DPPG/SR8: Three Gaussian band fitting parameters				
I	Amide I	1638 ± 0.4	20 ± 0.6	-0.0063
II	Lipid carbonyl	1724 ± 0.7	15 ± 1	-0.0039
III	Lipid carbonyl	1760 ± 1.4	15 ± 2.1	0.0019

S4. Calculation of Fresnel factors

HD-VSFG experiment with SSP polarization combination measures the YYZ component of the nonlinear susceptibility $\chi^{(2)}$ (i.e., $\chi^{(2)}_{YYZ}$). The corresponding experimentally obtained effective $\chi^{(2)}$, which we abbreviate as $\chi^{(2)}_{eff,SSP}$, is related to the $\chi^{(2)}_{YYZ}$ by the following equation:[1]

$$\chi^{(2)}_{eff,SSP} = L_{YY}(\omega_{SF})\, L_{YY}(\omega_1)\, L_{ZZ}(\omega_2)\, \sin\theta_2\, \chi^{(2)}_{YYZ} \qquad \text{(S1)},$$

where $L_{ii}(\omega)$ indicates the Fresnel factor corresponding to the incident (ω_1 and ω_2) and reflected (ω_{SF}) lights, and θ_2 is the incident angle of the ω_2 infrared light. Expressions for $L_{ii}(\omega)$ terms are well-known and they have been taken from the literature.[1]

In our heterodyne experiment, we measured the normalized $\chi^{(2)}_{eff,SSP}$. The resonantly enhanced SF signal reflected from the sample surface is divided by the nonresonant SF signal reflected from a quartz surface (which is measured separately and used as reference), for phase and amplitude calibration.[2] Accordingly, Eq. S1 can be rewritten as follows:

$$\chi^{(2)}_{eff,SSP} = \left[\frac{r_S^{air/D_2O}}{r_S^{air/quartz}}\right] \times \left[\frac{L_{YY}(\omega_{SF})\, L_{YY}(\omega_1)\, L_{ZZ}(\omega_2)\, \sin\theta_2\, \chi^{(2)}_{YYZ}}{L_{YY}^{quartz}(\omega_{SF}) L_{YY}^{quartz}(\omega_1) L_{XX}^{quartz}(\omega_2)\, \cos\theta_2 \left(\frac{\chi^{(2),quartz}_{xxx}}{\Delta k}\right)}\right] \qquad \text{(S2)},$$

where r_S denotes the reflectivity coefficient for the s-polarized ω_{SF} light at the air/D_2O and air/quartz interfaces. $L_{ii}^{quartz}(\omega)$ represents the corresponding Fresnel factors for air/quartz interface. $\chi^{(2),quartz}_{xxx}$ is the nonlinear susceptibility of the reference z-cut quartz, which is real and positive, and $(1/\Delta k)$ is the coherence length of the ω_{SF} light under the given experimental conditions.[3] The quantity $(\chi^{(2),quartz}_{xxx}/\Delta k)$ is considered as constant for simplification. Therefore, Eq. S2 can be expressed as:

$$\chi^{(2)}_{eff,SSP} = \left[\frac{r_S^{air/D_2O}}{r_S^{air/quartz}}\right] \times \left[\frac{L_{YY}(\omega_{SF})\, L_{YY}(\omega_1)\, L_{ZZ}(\omega_2)\, \sin\theta_2}{L_{YY}^{quartz}(\omega_{SF}) L_{YY}^{quartz}(\omega_1) L_{XX}^{quartz}(\omega_2)\, \cos\theta_2}\right] \times \chi^{(2)\prime}_{YYZ} \qquad \text{(S3)},$$

where $\chi^{(2)\prime}_{YYZ} = \frac{\chi^{(2)}_{YYZ}}{(\chi^{(2),quartz}_{xxx}/\Delta k)}$ in arbitrary unit.

Finally, after multiplying with all the Fresnel factors and reflectivity coefficients (see Table S3), we obtained the following relation:

$$\chi^{(2)}_{\mathrm{eff,SSP}} = 0.6974 \times \chi^{(2)'}_{\mathrm{YYZ}} \quad \text{(S4).}$$

Similarly, for PPP polarization combination, $\chi^{(2)}_{\mathrm{eff,PPP}}$ can be expressed as:[1]

$$\chi^{(2)}_{\mathrm{eff,PPP}} = \left[\frac{r_P^{\mathrm{air/D_2O}}}{r_P^{\mathrm{air/quartz}}}\right] \times \left[\frac{-L_{XX}(\omega_{SF})L_{XX}(\omega_1)L_{ZZ}(\omega_2)\cos\theta_{SF}\cos\theta_1\sin\theta_2\chi^{(2)}_{XXZ} + L_{ZZ}(\omega_{SF})L_{ZZ}(\omega_1)L_{ZZ}(\omega_2)\sin\theta_{SF}\sin\theta_1\sin\theta_2\chi^{(2)}_{ZZZ}}{L_{XX}^{\mathrm{quartz}}(\omega_{SF})L_{XX}^{\mathrm{quartz}}(\omega_1)L_{XX}^{\mathrm{quartz}}(\omega_2)\cos\theta_{SF}\cos\theta_1\cos\theta_2\left(\frac{\chi^{(2),\mathrm{quartz}}_{xxx}}{\Delta k}\right)}\right] \quad \text{(S5).}$$

In Eq. S5, we have ignored the contribution from $\chi^{(2)}_{XZX}$ and $\chi^{(2)}_{ZXX}$ (which also appear in $\chi^{(2)}_{\mathrm{eff,PPP}}$) components as they cancelled out each other because of the similar magnitudes and opposite signs of their coefficients.[4] Now, following a similar treatment to that of Eq. S3, the final form of the Eq. S5 is obtained as follows:

$$\chi^{(2)}_{\mathrm{eff,PPP}} = -0.5497\,\chi^{(2)'}_{\mathrm{XXZ}} + 0.2570\,\chi^{(2)'}_{\mathrm{ZZZ}} \quad \text{(S6),}$$

where $\chi^{(2)'}_{\mathrm{XXZ}} = \frac{\chi^{(2)}_{\mathrm{XXZ}}}{(\chi^{(2),\mathrm{quartz}}_{\mathrm{xxx}}/\Delta k)}$ and $\chi^{(2)'}_{\mathrm{ZZZ}} = \frac{\chi^{(2)}_{\mathrm{ZZZ}}}{(\chi^{(2),\mathrm{quartz}}_{\mathrm{xxx}}/\Delta k)}$ in arbitrary unit.

As $\chi^{(2)}_{\mathrm{XXZ}}$ and $\chi^{(2)}_{\mathrm{YYZ}}$ components are equivalent in our HD-VSFG measurement, Eq. S6 can be rewritten as:

$$\chi^{(2)}_{\mathrm{eff,PPP}} = -0.5497\,\chi^{(2)'}_{\mathrm{YYZ}} + 0.2570\,\chi^{(2)'}_{\mathrm{ZZZ}} \quad \text{(S7).}$$

Equation S4 and Eq. S7 are used to extract the YYZ and ZZZ spectral components of $\mathrm{Im}\chi^{(2)}$ (i.e., $\mathrm{Im}\chi^{(2)'}_{\mathrm{YYZ}}$ and $\mathrm{Im}\chi^{(2)'}_{\mathrm{ZZZ}}$) from polarization dependent experimental data. Notably, the coefficient for $\chi^{(2)'}_{\mathrm{YYZ}}$ measured in PPP polarization combination is negative (Eq. S7) and it has larger magnitude than that of the $\chi^{(2)'}_{\mathrm{ZZZ}}$, making the overall sign of $\mathrm{Im}\chi^{(2)}_{\mathrm{eff,PPP}}$ negative. This explains the sign flip of the $\mathrm{Im}\chi^{(2)}_{\mathrm{eff,PPP}}$ spectra shown in Fig. 5 (a and b) of the main text.

Table S3. List of required Fresnel factors and reflectivity coefficients.

	$L_{XX}(\omega_1)$	$L_{YY}(\omega_1)$	$L_{ZZ}(\omega_1)$		
Air/D_2O	0.9144	0.8075	0.8264		
Air/Quartz	0.8565	0.7213	-		
	$L_{XX}(\omega_2)$	$L_{YY}(\omega_2)$	$L_{ZZ}(\omega_2)$		
Air/D_2O	-	0.8145	0.8330		
Air/Quartz	0.9329	-	-		
	$L_{XX}(\omega_{SF})$	$L_{YY}(\omega_{SF})$	$L_{ZZ}(\omega_{SF})$	$\lvert r_S(\omega_{SF})\rvert$	$\lvert r_P(\omega_{SF})\rvert$
Air/D_2O	0.9151	0.8058	0.8250	0.1942	0.0867
Air/Quartz	0.8573	0.7192	-	0.2808	0.1445

Table S4. List of parameters which are used for calculating Fresnel factors and reflectivity coefficients.

	ω_1	ω_2	ω_{SF}
λ (nm)	795	5857.9	700
ω (cm^{-1})	12578.6	1707.1	14285.7
n_{D2O}	1.3241	1.2719	1.3256
n_{Quartz}	1.5385	1.3304	1.5407
n_{Air}	1	1	1
θ^i_{Air}	37°	42°	37.30°
θ^r_{D2O}	27.03°	31.74°	27.20°
θ^r_{Quartz}	23.03°	30.19°	23.16°

θ^i and θ^r indicates the angle of incidence and angle of refraction, respectively.

n corresponds to the refractive index.[5]

S5. Spectral components of $\chi^{(2)}$ tensor with Gaussian fitting analysis

Heterodyne detection provides the imaginary part of $\chi^{(2)}_{\mathrm{eff,SSP}}$ (or $\chi^{(2)}_{\mathrm{eff,PPP}}$) i.e., $\mathrm{Im}\chi^{(2)}_{\mathrm{eff,SSP}}$ (or $\mathrm{Im}\chi^{(2)}_{\mathrm{eff,PPP}}$). We obtained the $\mathrm{Im}\chi^{(2)'}_{\mathrm{YYZ}}$ and $\mathrm{Im}\chi^{(2)'}_{\mathrm{ZZZ}}$ spectral components (shown in Fig. S3) from the polarization dependent experimental data using the following equations, obtained from Eq. S4 and Eq. S7:

$$\mathrm{Im}\chi^{(2)'}_{\mathrm{YYZ}} = \mathrm{Im}\chi^{(2)}_{\mathrm{eff,SSP}}/0.6974 \quad \text{(S8)},$$

$$\mathrm{Im}\chi^{(2)'}_{\mathrm{ZZZ}} = (\mathrm{Im}\chi^{(2)}_{\mathrm{eff,PPP}} + 0.5497\ \mathrm{Im}\chi^{(2)'}_{\mathrm{YYZ}})/0.2570 \quad \text{(S9)}.$$

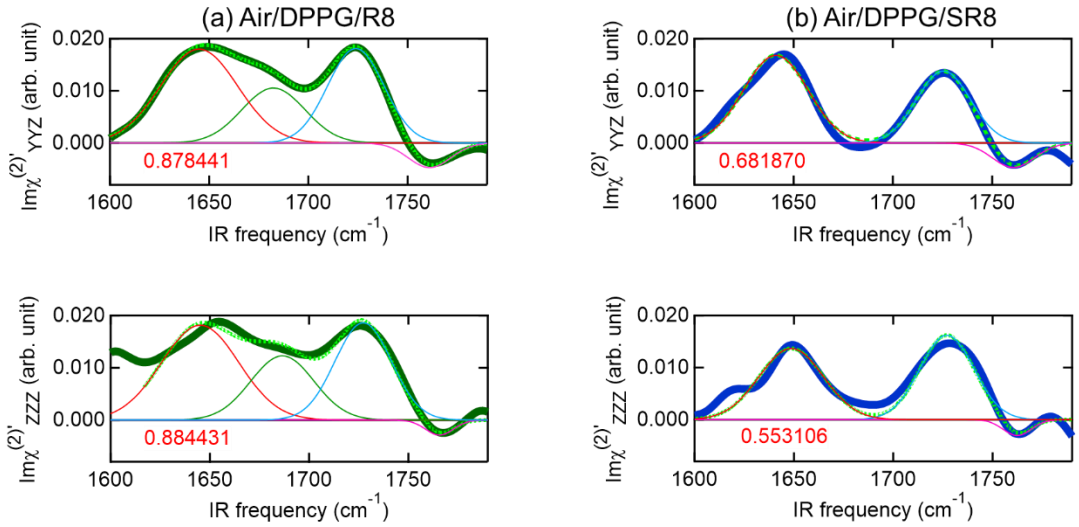

Figure S3. $\mathrm{Im}\chi^{(2)'}_{\mathrm{YYZ}}$ (top panel) and $\mathrm{Im}\chi^{(2)'}_{\mathrm{ZZZ}}$ (bottom panel) spectra for (a) air/DPPG/R8 (thick green lines) and (b) air/DPPG/SR8 (thick blue lines) interfaces. The obtained spectra were fitted with four or three Gaussian sub-bands, in a manner similar to that described in Section S3. The fitted spectra are shown with broken green lines. Individual Gaussian components are also shown with thin solid lines. The area-integrated amplitudes of the amide I band corresponding to the α-helix component of the peptides (thin red) are indicated below the respective bands.

S6. Orientational angle calculation and simulation of $\chi^{(2)}$ angular distribution

To calculate the orientational angle corresponding to the tilt of the helical components of R8 and SR8 with respect to the surface normal, the experimental amplitude ratio between $\mathrm{Im}\chi^{(2)'}_{YYZ}$ and $\mathrm{Im}\chi^{(2)'}_{ZZZ}$ is used. The $\chi^{(2)}$ amplitude ratio is related to the orientational angle by the following well-known equations:[6]

$$\chi^{(2)}_{YYZ} = \frac{1}{2}N_s[(1+R)\langle\cos\theta\rangle - (1-R)\langle\cos^3\theta\rangle]\beta_{ccc} \quad \text{(S10)}$$

$$\chi^{(2)}_{ZZZ} = N_s[R\langle\cos\theta\rangle + (1-R)\langle\cos^3\theta\rangle]\beta_{ccc} \quad \text{(S11)}$$

$$\frac{\chi^{(2)}_{ZZZ}}{\chi^{(2)}_{YYZ}} = \frac{2[R\,\langle\cos\theta\rangle+(1-R)\langle\cos^3\theta\rangle]}{[(1+R)\langle\cos\theta\rangle-(1-R)\langle\cos^3\theta\rangle]} \quad \text{(S12),}$$

where $R = \beta_{aac}/\beta_{ccc}$ (β; molecular hyperpolarizability). N_s is the surface number density. (X, Y, Z) and (a, b, c) correspond to the laboratory coordinate and molecular coordinate systems, respectively. The molecular c-axis is parallel to the helical axis (see Fig. S5) of the α-helix components of the two peptides. Orientational angle θ is the angle between the molecular c-axis and the laboratory Z-axis (which is also the surface normal) and $\langle\ \ \rangle$ indicates the ensemble averaging. The orientational distributions, $\langle\cos\theta\rangle$ and $\langle\cos^3\theta\rangle$ are expressed as follows:[7]

$$\langle\cos\theta\rangle = \frac{\int_0^\pi \cos\theta\, \exp\left[\frac{-(\theta-\theta_0)^2}{2\sigma^2}\right]\sin\theta\, d\theta}{\int_0^\pi \exp\left[\frac{-(\theta-\theta_0)^2}{2\sigma^2}\right]\sin\theta\, d\theta} \quad \text{(S13)}$$

$$\langle\cos^3\theta\rangle = \frac{\int_0^\pi \cos^3\theta\, \exp\left[\frac{-(\theta-\theta_0)^2}{2\sigma^2}\right]\sin\theta\, d\theta}{\int_0^\pi \exp\left[\frac{-(\theta-\theta_0)^2}{2\sigma^2}\right]\sin\theta\, d\theta} \quad \text{(S14).}$$

Here, σ is the width of the Gaussian function. In case of δ function distribution of tilt angle, $\langle\cos\theta\rangle = \cos\theta$ and $\langle\cos^3\theta\rangle = \cos^3\theta$.

For simplicity, the A-type (totally symmetric) vibrational mode of helical structure is considered as the dominant component.[6] The value of R=0.54 is used for calculation.[6]

Using Eq. S12, the angular distribution of $\chi^{(2)}$ amplitude ratio for θ ranging from 0-90° is simulated, assuming various orientational distribution widths. The simulated $\chi^{(2)}_{ZZZ}/\chi^{(2)}_{YYZ}$ for helical component of amide I band is shown in Fig. 7 of the main text.

To obtain the experimental values of $\chi^{(2)}_{ZZZ}/\chi^{(2)}_{YYZ}$, the experimental $\mathrm{Im}\chi^{(2)\prime}_{YYZ}$ and $\mathrm{Im}\chi^{(2)\prime}_{ZZZ}$ spectra of the air/DPPG/R8 and air/DPPG/SR8 interfaces were fitted with multiple Gaussian functions (see Fig. S3 of previous section). The area integrated amplitudes of the component Gaussian band ~1640 cm^{-1} (for helical structure) are used to calculate $\mathrm{Im}\chi^{(2)\prime}_{ZZZ}/\mathrm{Im}\chi^{(2)\prime}_{YYZ}$. The θ can be evaluated from the intersection point between the experimentally obtained $\mathrm{Im}\chi^{(2)\prime}_{ZZZ}/\mathrm{Im}\chi^{(2)\prime}_{YYZ}$ value and the simulated curve. The θ values obtained for the δ function distribution are tabulated in Table 1 of the main text.

We have also simulated $\chi^{(2)}_{ZZZ}/\chi^{(2)}_{YYZ}$ for the major lipid carbonyl band (Fig. S4a) using Eq. S12 by putting R=0.13.[6] Similarly, $\chi^{(2)}_{SSP}$ and $\chi^{(2)}_{PPP}$ for lipid C=O bonds (Fig. 8 in the main text) as well as $\chi^{(2)}_{PPP}/\chi^{(2)}_{SSP}$ (Fig. S4b) are simulated using Eq. S4 & Eq. S7, and Eq. S10 & Eq. S11, with R=0.13.[6]

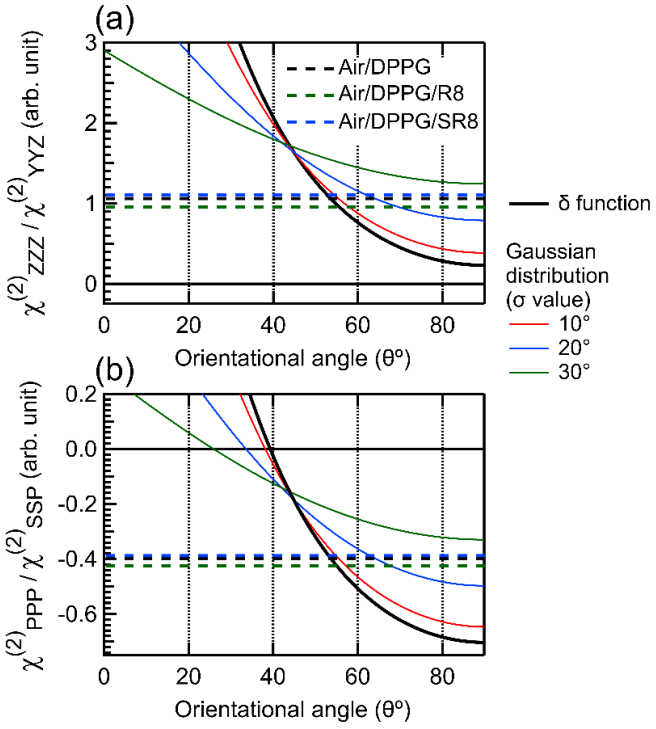

Figure S4. Simulated (a) $\chi^{(2)}_{ZZZ}/\chi^{(2)}_{YYZ}$, and (b) $\chi^{(2)}_{PPP}/\chi^{(2)}_{SSP}$ for the major C=O band of the lipid. Broken horizontal lines indicate the amplitude ratio obtained from the experimental data, in the presence or the absence of CPPs. The experimental amplitude ratios for the major lipid C=O band (i.e.,1720 cm^{-1} region) are obtained from the maximum peak amplitudes of $\mathrm{Im}\chi^{(2)\prime}_{YYZ}$ and $\mathrm{Im}\chi^{(2)\prime}_{ZZZ}$ (or $\mathrm{Im}\chi^{(2)}_{eff,SSP}$ and $\mathrm{Im}\chi^{(2)}_{eff,PPP}$) spectra without any fitting analysis.

S7. Probable configuration of SR8

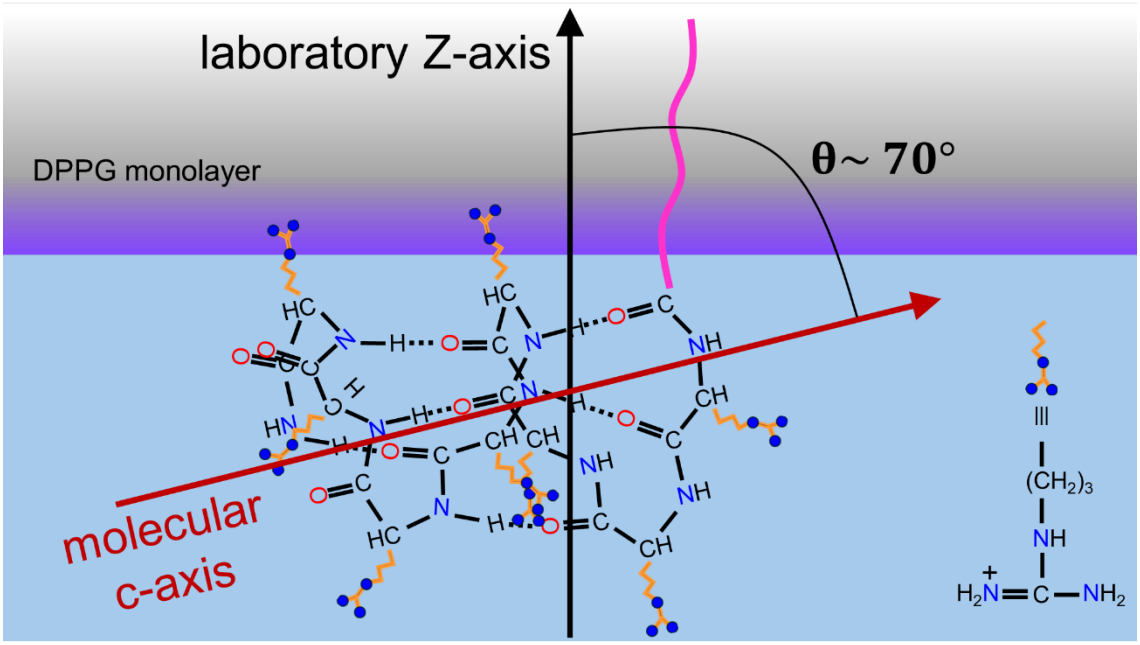

Figure S5. The schematic of a probable configuration of SR8 at the air/DPPG/10mM Tris-HCl buffer (pD 7.4, D_2O) interface.

S8. Peak frequencies of lipid carbonyl bands

Table S5. Lipid carbonyls stretch frequencies of the $Im\chi^{(2)}_{eff,SSP}$ and $Im\chi^{(2)}_{eff,PPP}$ spectra from air/DPPG, air/DPPG/R8, and air/DPPG/SR8 interfaces. The values correspond to the peak maxima of the respective bands which are obtained without fitting.

$Im\chi^{(2)}_{eff,SSP}$	Major positive band (cm^{-1})	Minor negative band (cm^{-1})
Air/DPPG	1721.3	1755.7
Air/DPPG/R8	1723.9	1762
Air/DPPG/SR8	1725.2	1760.8
$Im\chi^{(2)}_{eff,PPP}$	Major positive band (cm^{-1})	Minor negative band (cm^{-1})
Air/DPPG	1720.1	1751.9
Air/DPPG/R8	1722.6	1757
Air/DPPG/SR8	1723.9	1757

S9. References

1. X. Zhuang, P. B. Miranda, D. Kim and Y. R. Shen, Phys. Rev. B, 1999, **59**, 12632-12640.
2. S. Nihonyanagi, S. Yamaguchi and T. Tahara, J. Chem. Phys., 2009, **130**, 204704.
3. X. Wei, S.-C. Hong, A. I. Lvovsky, H. Held and Y. R. Shen, J. Phys. Chem. B, 2000, **104**, 3349-3354.
4. S. Sun, F. Tang, S. Imoto, D. R. Moberg, T. Ohto, F. Paesani, M. Bonn, E. H. G. Backus and Y. Nagata, Phys. Rev. Lett., 2018, **121**, 246101.
5. M. N. Polyanskiy, Sci. Data, 2024, **11**, 94.
6. J. Wang, S.-H. Lee and Z. Chen, J. Phys. Chem. B, 2008, **112**, 2281-2290.
7. W. Gan, D. Wu, Z. Zhang, R.-r. Feng and H.-f. Wang, J. Chem. Phys., 2006, **124**, 114705.